Convolution-based interferometric redatuming of source and receivers in a heterogeneous medium

D. F. Barrera P.*, Jörg Schleicher†, J. van der Neut‡ and K. Wapenaar‡

*DEP/UNICAMP & INCT-GP, †IMECC/UNICAMP & INCT-GP and ‡Delft University of Technology

Abstract

Seismic interferometry is defined as the method to redatum sources and receivers where there only are receivers or sources, respectively. This can be done by correlation- or convolution-based methods. In this work we will present a new approach to reposition the seismic array over the earth's surface to an arbitrary datum at depth in two steps using deconvolution-based methods: (a) redatuming of receivers and (b) redatuming of sources. This methodology accounts for inhomogeneities in the overburden medium to remove anticausal events.

Introduction

Seismic interferometry is a technique that allows to retrieve the Green's functions for sources at positions where only receivers are available (or vice versa). The classic redatuming procedure correlates surface seismic data with those acquired at depth. This correlation-based method has been well studied in the literature, by Wapenaar et al. (2008), Schuster (2009) Curtis (2009), Wapenaar et al. (2010), van der Neut (2012), etc.

Seismic interferometry by convolution is an alternative to the classical correlation-based scheme. Are many situations where it is more convenient than correlation methods. One of the main advantages of the convolution-based procedure is its inherent compensation for the properties of the source wavelet. Another important advantage is that the underlying theory does not require the assumtion of a lossless medium (Slob and Wapenaar, 2007).

In this work, we combine convolution-based interferometry with inverse wavefield extrapolation to derive an alternative procedure for retrieving the total wavefield at the datum. Inverse wavefield extrapolation is a concept used to describe the process of retrieving the focusing functions at an arbitrary datum by means of retropropagation of the wavefield recorded at the earth's surface (van der Neut et al., 2015).

In our proposed procedure, we use a convenient form of inverse wavefield extrapolation to determine the upward propagating Green's function at the datum for a point source at the earth's surface. This upgoing Green's function is then used to retrieve the primary-reflected wavefield at the datum, using this new approach, we reduced influence of the overburden in the form of multiples, spurious events of the Green's functions, and anticausal events. The only required information for the proposed technique is a velocity model of the datum overburden. This model is used to simulate the vertical derivative of the transmitted wavefield to the datum and the truncated overburden-scattered wavefield at the surface.

Redatuming of receivers

We consider two states A and B in the Helmholtz equation in order to calculate the reciprocity theorem of the convolution type. We assume that both states have the same properties, i.e., $\rho^A(x) = \rho^B(x) = \rho(x)$ and $c^A(x) = c^B(x) = c(x)$. Since the states differ only in the source, corresponding wavefields p^A and p^B must satisfy

$$\rho(x)\nabla\cdot\left[\frac{1}{\rho(x)}\nabla\hat{p}^A\right]+\frac{\omega^2}{c^2(x)}\hat{p}^A = -\hat{S}^A, \quad (1)$$

$$\rho(x)\nabla\cdot\left[\frac{1}{\rho(x)}\nabla\hat{p}^B\right]+\frac{\omega^2}{c^2(x)}\hat{p}^B = -\hat{S}^B, \quad (2)$$

Here $\rho(x)$ denotes the variable density, $\hat{p}$ the pressure field, $c(x)$ is the spatially varying wave velocity and $\hat{S}(x,\omega)$ is a source term. From equations (1) and (2) we deduced the reciprocity theorem of convolution type as

$$\oint\!\!\!\!\!\!\int_S \frac{1}{\rho(x)}\left(\hat{p}^B\nabla\hat{p}^A-\hat{p}^A\nabla\hat{p}^B\right)\cdot\hat{n}ds = \iiint_V \frac{1}{\rho(x)}\left(\hat{p}^A\hat{S}^B-\hat{p}^B\hat{S}^A\right)dv. \quad (3)$$

This equality is independent of the actual shape of volume V. Considering that are no sources inside at the volume V, the right-hand of equation (3) vanish. To analyze the closed-surface integral, we consider a cylindrical shape, where the surface S is decomposed into three parts. Invoking the Sommerfeld radiation conditions, we note that at infinite radius, the integral over the cylinder mantle will not contribute. (Schuster, 2009). Denoting the top and bottom parts of the cylinder surface as S_1 and S_2, respectively, to zero using Sommerfeld radiation condition we can rewrite expression (3) as

$$\iint_{S_1}\frac{1}{\rho(x)}(\hat{p}^B\nabla\hat{p}^A-\hat{p}^A\nabla\hat{p}^B)\cdot\hat{n}_1dx_1dx_2 = -\iint_{S_2}\frac{1}{\rho(x)}(\hat{p}^B\nabla\hat{p}^A-\hat{p}^A\nabla\hat{p}^B)\cdot\hat{n}_2dx_1dx_2. \quad (4)$$

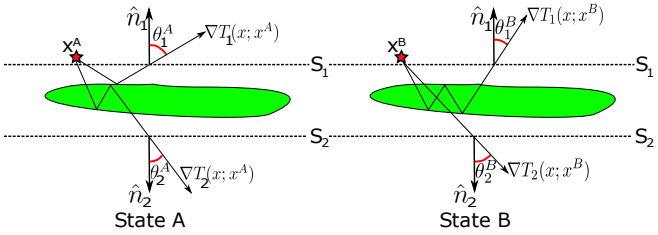

Figure 1: Sketch of two sources at positions x^A and x^B just above the surface S_1. Also shown at the receiver position x are the propagation directions of the incoming waves from x^A and x^B and their angles θ^A and θ^B with respect to the unit normal vector $\hat{n}$ to the surface.

One-way reciprocity theorem of convolution type

To deduce the one-way reciprocity theorems, we consider the two states, A and B, to represent the situations in Figure 1. In both states, we allow for an arbitrary inhomogeneous medium between the two surfaces, which are defined as $S_1 = \{(x_1,x_2,x_3) \in \mathbb{R}^2 | x_3 = x_3^1\}$ and $S_2 = \{(x_1,x_2,x_3) \in \mathbb{R}^2 | x_3 = x_3^2\}$. Note that we do not consider S_1 to be a free surface. States A and B differ in source distribution, with their sources located in x^A and x^B, respectively, and the receivers along both surfaces.

According to Wapenaar and Berkhout (1989) the total wave field can be decomposed in down- $(+)$ and up-going $(-)$ constituents, as

$$\hat{p}(x,\omega) = \hat{p}_+(x,\omega) + \hat{p}_-(x,\omega). \tag{5}$$

Substitution of decomposition (5) in expression (4) yields

$$\begin{aligned}
&\iint_{S_1} \frac{1}{\rho(x)} \Bigg[\left(\hat{p}_+^B + \hat{p}_-^B\right) \nabla \left(\hat{p}_+^A + \hat{p}_-^A\right) - \\
&\left(\hat{p}_+^A + \hat{p}_-^A\right) \nabla \left(\hat{p}_+^B + \hat{p}_-^B\right) \Bigg] \cdot \hat{n}_1 dx_1 dx_2 = \\
&- \iint_{S_2} \frac{1}{\rho(x)} \Bigg[\left(\hat{p}_+^B + \hat{p}_-^B\right) \nabla \left(\hat{p}_+^A + \hat{p}_-^A\right) - \\
&\left(\hat{p}_+^A + \hat{p}_-^A\right) \nabla \left(\hat{p}_+^B + \hat{p}_-^B\right) \Bigg] \cdot \hat{n}_2 dx_1 dx_2.
\end{aligned} \tag{6}$$

Assuming that the medium is smooth in a small region around S_1 and S_2, the main contributions to the integrals in equation (6) come from stationary points on surfaces S_1 and S_2. At those points the absolute cosines of the ray angles for $\hat{p}^A$ and $\hat{p}^B$ are identical. This implies, for example, that the terms $\hat{p}_+^B \nabla \hat{p}_-^A$ and $-\hat{p}_-^A \nabla \hat{p}_+^B$ give equal contribution to the integral, whereas the contributions of $-\hat{p}_+^B \nabla \hat{p}_+^A$ and $\hat{p}_+^A \nabla \hat{p}_+^B$ cancel each other (Wapenaar and Fokkema, 2006). Hence, we can rewrite equation (6) as

$$\begin{aligned}
&\iint_{S_1} \frac{1}{\rho(x)} \left(\hat{p}_+^B \nabla \hat{p}_-^A + \hat{p}_-^B \nabla \hat{p}_+^A\right) \cdot \hat{n}_1 dx_1 dx_2 = \\
&- \iint_{S_2} \frac{1}{\rho(x)} \left(\hat{p}_+^B \nabla \hat{p}_-^A + \hat{p}_-^B \partial_3 \hat{p}_+^A\right) \cdot \hat{n}_2 dx_1 dx_2.
\end{aligned} \tag{7}$$

Considering that the normal vectors at surfaces S_1 and S_2 are $\hat{n}_1 = (0,0,-1)$ and $\hat{n}_2 = (0,0,1)$, respectively. After

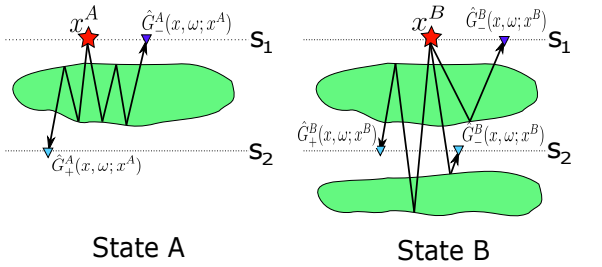

Figure 2: Two states with the same inhomogeneous medium between surfaces S_1 and S_2. State A describes the transmitted wavefield from S_1 to S_2 and its scattered response recorded at S_1, if the medium is homogeneous above S_1 and below S_2. State B describes the corresponding wavefields if the medium is also inhomogeneous below S_2.

previous procedure, we write in both sides of the equation (7) the term $\hat{p}_+^B \partial_3 \hat{p}_-^A$ as $-\hat{p}_-^A \partial_3 \hat{p}_+^B$, that is the most convenient form for our deductions at the next section of this work. We can recast equation (7) into the form

$$\begin{aligned}
&\iint_{S_1} \frac{1}{\rho(x)} \left[(-\partial_3 \hat{p}_+^B)\hat{p}_-^A + \hat{p}_-^B \partial_3 \hat{p}_+^A\right] dx_1 dx_2 = \\
&\iint_{S_2} \frac{1}{\rho(x)} \left[(-\partial_3 \hat{p}_+^B)\hat{p}_-^A + \hat{p}_-^B \partial_3 \hat{p}_+^A\right] dx_1 dx_2.
\end{aligned} \tag{8}$$

Upgoing Green's function

Let us now consider that in State A, the point source for a down-going wave field is located immediately above S_1, creating a delta function in the lateral coordinates at S_1. Then, according to Wapenaar et al. (2014), the derivative of the pressure field can be expressed as $\partial_3 \hat{p}_+^A = -\frac{1}{2}\delta(x - x^A)$. Moreover, we consider that in State A, all inhomogeneities are restricted to the medium between S_1 and S_2, i.e., above S_1 and below S_2, there are two homogeneous halfspaces (Figure 2).

In State B, we consider the same inhomogeneous medium between surfaces S_1 and S_2. Again, the medium above S_1 is homogeneous. However, above S_2 we consider now an arbitrary inhomogeneous medium. As in State A, we again consider a point source for a downgoing wave field just above the surface S_1, such that $\partial_3 \hat{p}_+^B = -\frac{1}{2}\delta(x - x^B)$. Of course the wavefields of both states admit decomposition according to equation (5). A detailed analysis of the propagating wavefield constituents in both states at both surfaces results in the overview presented in Table 1.

Surface	Direction	State A	State B
S_1	+	point source in x^A	point source in x^B
S_1	-	$\hat{G}_-^A(x,\omega;x^A)$	$\hat{G}_-^B(x,\omega;x^B)$
S_2	+	$\hat{G}_+^A(x',\omega;x^A)$	$\hat{G}_+^B(x',\omega;x^B)$
S_2	-	0	$\hat{G}_-^B(x',\omega;x^B)$

Table 1: Wavefield responses at surfaces S_1 and S_2 in the states A and B, respectively.

Substitution of the expressions of Table 1 in the one-way reciprocity theorem of convolution type (equation 8) allows

to simplify the latter to

$$\frac{1}{2\rho(x^A)}\hat{G}^B_-(x^A,\omega;x^B)-\frac{1}{2\rho(x^B)}\hat{G}^A_-(x^B,\omega;x^A)= -\iint_{S_2}\frac{1}{\rho(x)}\hat{G}^B_-(x',\omega;x^B)\partial_3\hat{G}^A_+(x',\omega;x^A)d^2x', \tag{9}$$

where we have also used that the vertical wavefield derivatives at the point sources are given by delta functions as mentioned above. Equation (9) is an expression that allows for least-squares inversion to retrieve the up-going Green's function $\hat{G}^B_-(x',\omega;x^B)$ in State B (i.e., for the complete inhomogeneous medium) if we know the terms $\frac{1}{2\rho(x^B)}\hat{G}^A_-(x^B,\omega;x^A)$ and $\frac{1}{\rho(x)}\partial_3\hat{G}^A_+(x',\omega;x^A)$ in State A, which use only a model of the inhomogeneities in between the surfaces S_1 and S_2.

Redatuming of sources

The Helmholtz equations describing the wavefields for a point source at x^B in states A and B that corresponds to the background and perturbed mediums, respectively. It is written as

$$\mathscr{L}^A\hat{G}^A(x,\omega;x^B)=-\delta(x-x^B) \tag{10}$$

and

$$\mathscr{L}^B\hat{G}^B(x,\omega;x^B)=-\delta(x-x^B). \tag{11}$$

where the associated Helmholtz operators are

$$\mathscr{L}^A=\rho_A(x)\nabla\cdot\left[\frac{1}{\rho_A(x)}\nabla\right]+\frac{\omega^2}{c_A^2(x)}, \tag{12}$$

and

$$\mathscr{L}^B=\rho_B(x)\nabla\cdot\left[\frac{1}{\rho_B(x)}\nabla\right]+\frac{\omega^2}{c_B^2(x)}. \tag{13}$$

Here, $\rho_A(x)$, $\rho_B(x)$ and $c_A(x)$, $c_B(x)$ are the density and velocity in the unperturbed and perturbed media, respectively.

There is a unique difference wavefield $\hat{G}^s(x,\omega;x^B)$, conventionally also known as scattered wavefield (Bleistein et al., 2001), that allows to relate the two Green's functions of states A and B as

$$\hat{G}^B(x,\omega;x^B)=\hat{G}^A(x,\omega;x^B)+\hat{G}^s(x,\omega;x^B). \tag{14}$$

It is our objective to determine this scattered wavefield due to the presence of inhomogeneities below S_2 as if recorded with sources and receivers at S_2.

Upon the use of the general form of the *perturbation operator* or *scattering potential*, defined as (Rodberg and Thaler, 1967)

$$\mathscr{V}=\mathscr{L}^B-\mathscr{L}^A, \tag{15}$$

and the wavefield decomposition (14), equation (11) can be represented as

$$\left(\mathscr{L}^A+\mathscr{V}\right)\left[\hat{G}^A(x,\omega;x^B)+\hat{G}^s(x,\omega;x^B)\right]=-\delta(x-x^B). \tag{16}$$

Together with equation (10), this leads to

$$\mathscr{L}^A\hat{G}^s(x,\omega;x^B)=-\mathscr{V}\left[\hat{G}^A(x,\omega;x^B)+\hat{G}^s(x,\omega;x^B)\right]. \tag{17}$$

At this point, we consider a Green's function $\hat{G}^A(x,\omega;x')$, which satisfies a Helmholtz equation similar to equation (10), however with a point source at x'. Multiplication of this Helmholtz equation with $\hat{G}^s(x,\omega;x^B)$ yields

$$\rho_A(x)\hat{G}^s(x,\omega;x^B)\nabla\cdot\left[\frac{1}{\rho_A(x)}\nabla\hat{G}^A(x,\omega;x')\right]+ \frac{\omega^2}{c_A^2(x)}\hat{G}^s(x,\omega;x^B)\hat{G}^A(x,\omega;x')=-\hat{G}^s(x,\omega;x^B)\delta(x-x'), \tag{18}$$

Correspondingly, multiplying in both sides of equation (17) by $\hat{G}^A(x,\omega;x')$, we can explicitly write

$$\rho_A(x)\hat{G}^A(x,\omega;x')\nabla\cdot\left[\frac{1}{\rho_A(x)}\nabla\hat{G}^s(x,\omega;x^B)\right]+ \frac{\omega^2}{c_A^2(x)}\hat{G}^A(x,\omega;x')\hat{G}^s(x,\omega;x^B)= -\hat{G}^A(x,\omega;x')\mathscr{V}\left[\hat{G}^A(x,\omega;x^B)+\hat{G}^s(x,\omega;x^B)\right]. \tag{19}$$

Subtracting equation (19) from (18) and rewriting the terms, we find

$$\nabla\cdot\left\{\frac{1}{\rho_A(x)}\left[\hat{G}^A(x,\omega;x')\nabla\hat{G}^s(x,\omega;x^B)- \hat{G}^s(x,\omega;x^B)\nabla\hat{G}^A(x,\omega;x')\right]\right\}= \frac{1}{\rho_A(x)}\left[\hat{G}^A(x,\omega;x')\mathscr{V}\hat{G}^B(x,\omega;x^B)-\hat{G}^s(x,\omega;x^B)\delta(x-x')\right]. \tag{20}$$

After application of Green's theorem, solving the volume integral of the term with the delta function, and reorganizing expression (20), we arrive at

$$\hat{G}^s(x',\omega;x^B)= \rho_A(x')\left\{\iiint_V\frac{1}{\rho_A(x)}\hat{G}^A(x,\omega;x')\mathscr{V}\hat{G}^B(x,\omega;x^B)dV- \oiint_S\frac{1}{\rho_A(x)}\left[\hat{G}^A(x,\omega;x')\nabla\hat{G}^s(x,\omega;x^B)- \hat{G}^s(x,\omega;x^B)\nabla\hat{G}^A(x,\omega;x')\right]\cdot\hat{n}\,dS\right\}. \tag{21}$$

Equation (21) represents the scattered Green's function with source in x^B and receiver in x'. It is given by the sum of a volume and a closed-surface integral, multiplied by the unperturbed density in x'. Considering that in both states A and B the overburden in between the surfaces S_1 and S_2 is the same, the scattering potential satisfies $\mathscr{V}=0$ inside V. Thus,

$$\iiint_V\frac{1}{\rho_A(x)}\hat{G}^A(x,\omega;x')\mathscr{V}\hat{G}^B(x,\omega;x^B)dV=0. \tag{22}$$

Equation (22) allows us to simplify the convolution-based interferometric equation (21) as an integral evaluated over the closed surface S. In analogy to the previous section, we divide the closed surface into three parts S_1, S_2 and S_3. Again, according to Schuster (2009) the Sommerfeld radiation conditions guarantee that the integral over S_3

vanishes at infinity. With the remaining integrals over surfaces S_1 and S_2 in equation (21), we have

$$\begin{aligned}\hat{G}^s(x',\omega;x^B) = \\ \rho_A(x')\Bigg\{\iint_{S_1}\frac{1}{\rho_A(x)}\Big[\hat{G}^A(x,\omega;x')\nabla\hat{G}^s(x,\omega;x^B)- \\ \hat{G}^s(x,\omega;x^B)\nabla\hat{G}^A(x,\omega;x')\Big]\cdot\hat{n}_1 dx_1 dx_2 + \\ \iint_{S_2}\frac{1}{\rho_A(x)}\Big[\hat{G}^A(x,\omega;x')\nabla\hat{G}^s(x,\omega;x^B)- \\ \hat{G}^s(x,\omega;x^B)\nabla\hat{G}^A(x,\omega;x')\Big]\cdot\hat{n}_2 dx_1 dx_2\Bigg\}.\end{aligned} \tag{23}$$

According to Wapenaar and Berkhout (1989), the wavefields in the above integrals can be decomposed into the up- and downward propagating constituents. Taking into account that the vectors are $\hat{n}_1 = (0,0,-1)$ and $\hat{n}_2 = (0,0,1)$, equation (23) can be written as

$$\begin{aligned}\hat{G}^s(x',\omega;x^B) = \\ 2\rho_A(x')\Bigg\{\iint_{S_1}\frac{1}{\rho_A(x)}\Big[\hat{G}^s_-(x,\omega;x^B)\partial_3\hat{G}^A_+(x,\omega;x')+ \\ \hat{G}^s_+(x,\omega;x^B)\partial_3\hat{G}^A_-(x,\omega;x')\Big]dx_1 dx_2 - \\ \iint_{S_2}\frac{1}{\rho_A(x)}\Big[\hat{G}^s_-(x,\omega;x^B)\partial_3\hat{G}^A_+(x,\omega;x')+ \\ \hat{G}^s_+(x,\omega;x^B)\partial_3\hat{G}^A_-(x,\omega;x')\Big]dx_1 dx_2\Bigg\},\end{aligned} \tag{24}$$

Since we consider a homogeneous halfspace above the nonfree surface S_1, there are no downward propagating wavefields at S_1. Therefore, the terms $\hat{G}^A_+(x,\omega;x')$ and $\hat{G}^s_+$ vanish at surface S_1 (see Figure 3), and the integral over surface S_1 is zero. Thus, equation (24) reduces to

$$\begin{aligned}\hat{G}^s(x',\omega;x^B) = \\ -2\rho_A(x')\iint_{S_2}\frac{1}{\rho_A(x)}\Big[\hat{G}^s_-(x,\omega;x^B)\partial_3\hat{G}^A_+(x,\omega;x')+ \\ \hat{G}^s_+(x,\omega;x^B)\partial_3\hat{G}^A_-(x,\omega;x')\Big]dx_1 dx_2\Bigg\}.\end{aligned} \tag{25}$$

In the integral over surface S_2, $\hat{G}^A_-(x,\omega;x')$ also vanishes, because in State A, the medium below S_2 is also homogeneous. Replacing x^B by x'', x' by x^B, and x by x', and invoking the reciprocity of the Green's functions.

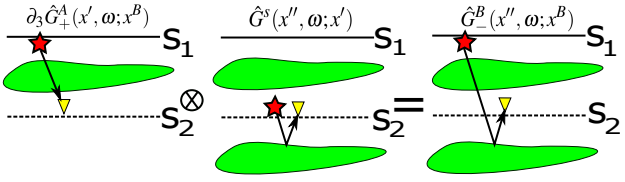

Figure 3: Sketch representing the geometrical situation in equation (26).

To make the link with the first step, we denote that $\hat{G}^s(x'',\omega;x^B) = \hat{G}^B_-(x'',\omega;x^B)$ for the given configuration. Therefore, equation (25) assumes its final form

$$\begin{aligned}\hat{G}^B_-(x'',\omega;x^B) = \\ -2\rho_A(x^B)\iint_{S_2}\frac{1}{\rho_A(x')}\hat{G}^s(x'',\omega;x')\partial_3\hat{G}^A_+(x',\omega;x^B)dx'_1 dx'_2.\end{aligned} \tag{26}$$

Equation (26) is the expression that describes convolution-based interferometric redatuming. If the scattering Green's function with source at the earth's surface and receivers at datum $\hat{G}^B_-(x'',\omega;x^B)$ is known, and we can model the vertical derivative of the incident Green's function $\partial_3\hat{G}^A_+(x',\omega;x^B)$, it is possible to retrieve by inversion the upward component of the scattering Green's function $\hat{G}^s(x'',\omega;x')$ with source and receivers at the datum. The situation is sketched in Figure 3.

Model

To validate above results we implemented equations (9) and (26) in a simple model of flat homogeneous layers. To further simplify things we consider the density in all layers constant. The model had a width of 5 km and depth of 1.5 km. The seismic array at the earth's surface (surface S_1) consisted of 201 shots and the same number of receivers for each shot, spaced at 25 m. The seismic array at the datum (at 500 m in depth) has the same source distribution as the one at the surface, and there are 201 receivers spaced at 25 m for each shot at the surface. Synthetic seismic data were simulated considering three situations: (1) shots and receivers are located at the surface (Figure 4a) in the full model, (2) shots are located at the surface and receivers at 500 m depth in the reference model using the exact overburden velocity field and a homogeneous halfspace below (Figure 4b), and (3) shots and receivers are located at the surface in the reference model (Figure 4c).

Results

The first step of redatuming consist in make reposition of the receivers of the seismic array at the earth's surface to the datum. For that step, we used equation (9). Input data are obtained from all of models of the Figure 4.

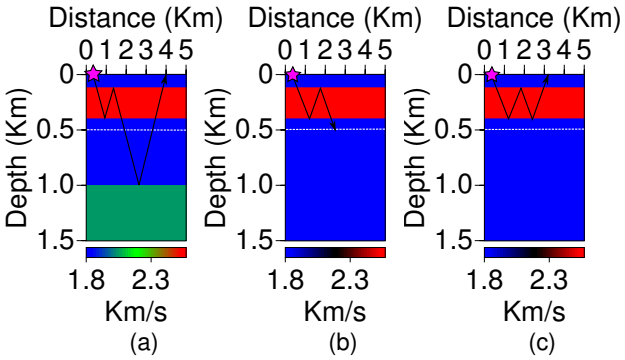

Figure 4: Modeling seismic data considering: (a) array of sources and receivers at the surface, (b) array of shots at the surface and receivers at 500 m depth and (c) array of sources and receivers at the surface in the overburden model.

The purpose is to retrieve the upward Green's function $\hat{G}^B_-(x',\omega;x^B)$ at 500 m in depth by damped least-squares inversion.

The principal aspect of the first step of our numerical inversion, i.e., the retrieval of the upward Green's functions, is that we actually invert a point spread function (PSF). Using a damped least-squares scheme to retrieve the inverse of the PSF, we tested different values of the regularization parameter ε in the inverse process. We used for ε four different percentage values with respect to the maximum value of the PSF. These percentages were: (1) 1%, (2) 0.1%, 0.01% and (4) 0.001%. The inversion results for these for values of ε are shown in Figure 5.

We note in Figure 5 that behind the principal primary reflection, marked with a red arrow, other events are visible, which are marked with green arrows. These later events are upgoing constituents of the wavefield, produced by overburden multiples (Barrera et al., 2016). Also, it is important to note that all responses retrieved by our inversion scheme do not include anticausal events. This is one of the main differences between the convolution-based procedure and conventional correlation-based interferometry.

Continuing the full redatuming procedure, we used the four different responses for the upward Green's functions of Figure 5 in the second step, that is, the redatuming of the sources to the datum, using equation (26). In other words, we retrieve the redatumed Green's function $\hat{G}^s_-(x'',\omega;x')$ using the now known downward Green's function $\hat{G}^s_+(x',\omega;x^B)$ (calculated in the first step) and the vertical derivative of the transmitted wavefield $\hat{G}^A_+(x',\omega;x^B)$. The result, using the four versions of the upward Green's function of Figure 5, is depicted in Figure 6.

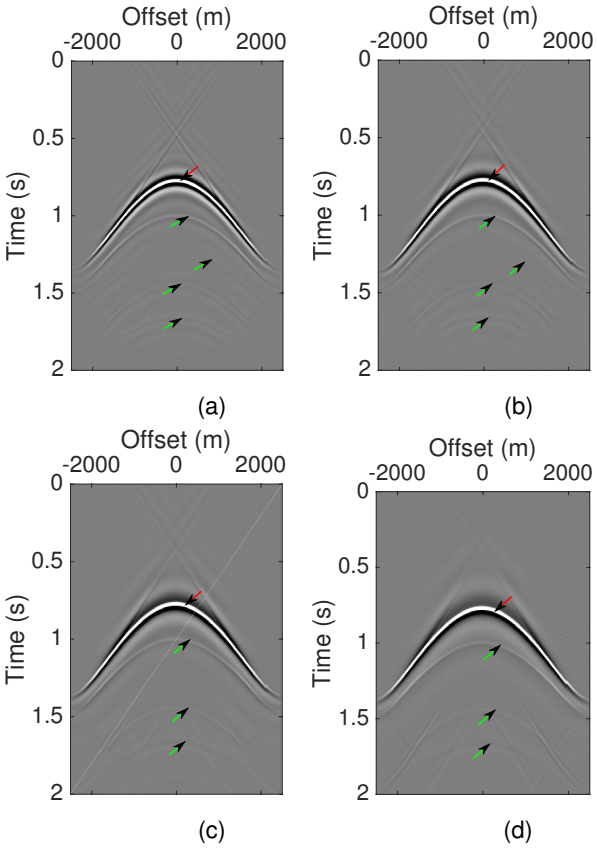

Figure 5: Upward responses obtained by the PSF inversion according to equation (9) with different values of ε: (a) 1%, (b) 0.1%, (c) 0.01% and (d) 0.001%.

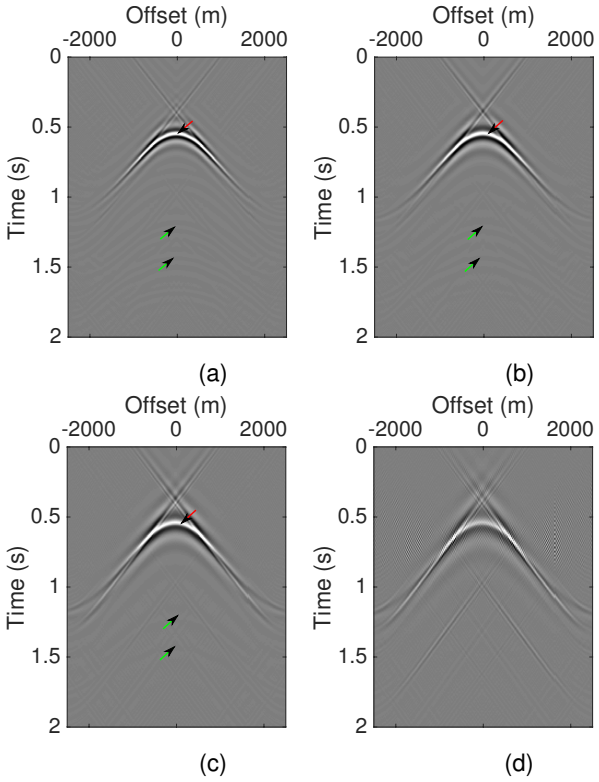

Figure 6: Redatuming responses of shot 101 with different values of ε in the PSF inversion: (a) 1%, (b) 0.1%, (c) 0.01% and (d) 0.001%.

We observe in Figure 6 that the redatumed wavefields recover the desired primary reflection event with slightly different quality. While the larger values of ε do a better job of suppressing artifacts, they also lead to a stronger damping of the desired wavefield at larger offsets. We notice a few traces of the the upgoing constituents from the overburden in the redatumed data. These are present, because we are inverting for the scattered field G^s instead of the true reflected field at the datum.

The quality of the inversion result as a function of the regularization parameter can be better assessed in Figure 7, which compares the central trace of each redatuming response to the modeled trace at the same location. While all events are kinematically nicely matched with the exact trace, we notice that the instabilities increase with decreasing ε. The artefacts that come from the instabilities at inversion can be attenuated by FK filters according with van der Neut and Wapenaar (2015).

Conclusions

In this work, we have derived a new scheme to calculate the upward Green's functions at a datum in depth. It makes use of an appropriate way for inverse wavefield

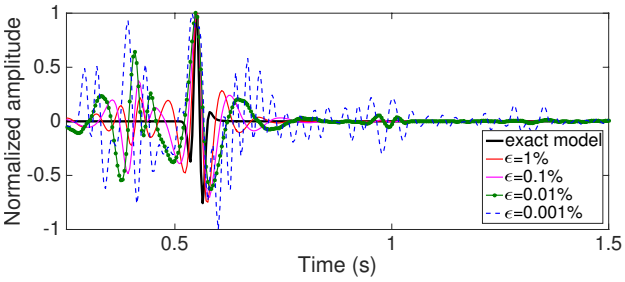

Figure 7: Central traces of the redatuming responses in the Figure 6 compared with the central trace of the exact model.

extrapolation. With this methodology it is possible to retrieve only the upward-propagating constituents at an arbitrary focusing surface without anticausal events and with reduced artifacts. The required input data are: (1) seismic reflection data from a seismic array over the earth's surface, (2) an earth model for the region between the surface and the datum. In this model, one needs to simulate the vertical derivative of the transmitted wavefield from the earth's surface until the datum and the truncated scattered wavefield of the overburden model with sources and receivers at the earth's surface.

Combining the upward Green's function retrieved by inverse wavefield extrapolation with the conventional scheme of interferometric redatuming by convolution-based methods, we were able to retrieve the primary-reflection event in a synthetic-data example using a simple synthetic velocity model. The redatuming responses had slight influences of the upward constituents associated to multiples in the overburden retrieved in the first step of the redatuming scheme. As a major advantage, there is no influence of anticausal events in the final responses, which were removed with the inverse wavefield extrapolation in the first step of the redatuming process.

The second step of the redatuming scheme presented here demonstrate that the reflection event from the interface below the datum was positioned correctly, and this response kept the correct amplitude proportions as compared to the corresponding data modeled at the datum level.

It is to be stressed that the equations solved in this work by means of damped least-squares inversion represent ill-posed problems. Therefore, the solution by inversion is very sensitive to small variations. Using different values of the regularization parameter, we noted that the quality of the results depend visibly on that parameter. While large values help to suppress unwanted effects, they also reduce the amplitudes of the desired events. The latter effect increases with offset.

Acknowledgments

We are grateful to the Brazilian agencies CNPq and FINEP, as well as Petrobras and the sponsors of the Wave Inversion Technology (WIT) Consortium for their support. The second author acknowledges a grant from the Santander Mobility Program.

References

Barrera, D. F., Schleicher, J., and van der Neut, J. (2016). Up- and down-going green's functions retrieved by inverse wavefield extrapolation. *WIT report*.

Bleistein, N., Cohen, J. K., and Jr., J. W. S. (2001). *Mathematics of Multidimensional Seismic Imaging, Migration, and Inversion*. Springer.

Curtis, A. (2009). Source-receiver seismic interferometry. *SEG meeting*, pages 3655–3659.

Rodberg, L. S. and Thaler, R. M. (1967). Introduction to the quantum theory of scattering. *Academic Press*.

Schuster, G. (2009). *Seismic interferometry*. Cambridge.

Slob, E. and Wapenaar, K. (2007). Electromagnetic green's functions retrieval by cross-correlation and cross-convolution in media with losses. *Geophysical Research Letters*, 4:L05307.

van der Neut, J. (2012). *Interferometric redatuming by multidimensional deconvolution*. PhD thesis, Delft University of Technology.

van der Neut, J. and Wapenaar, K. (2015). Point spread functions for intrferometric imaging. *Geophysical prospecting*, 63:1033–1049.

van der Neut, J., Wapenaar, K., Thorbecke, J., Slob, E., and Vasconcelos, I. (2015). An illustration of adaptative marchenko imaging. *The Leading Edge*, pages 818–822.

Wapenaar, C. P. A. and Berkhout, A. J. (1989). *Elastic Wave Field Extrapolation: Redatuming of Single- and Multi-Component Seismic Data*. Elsevier.

Wapenaar, K. and Fokkema, J. (2006). Green's function representations for seismic interferometry. *Geophysics*, 71:SI33–SI46.

Wapenaar, K., Ruigrok, E., van der Neut, J., Draganov, D., Hunziker, J., Slob, E., and Thorbecke, J. (2010). Green's function representation for seismic interferometry by deconvolution. *SEG meeting*, pages 3972–3978.

Wapenaar, K., Slob, E., and Snieder, R. (2008). Seismic and electromagnetic controlled-source interferometry in dissipative media. *Geophysical prospecting*, 56:419 – 434.

Wapenaar, K., Thorbecke, J., van der Neut, J., Broggini, F., Slob, E., and Snieder, R. (2014). Green's function retrieval from reflection data, in absence of receiver at the virtual source position. *The Journal of the Acoustical Society of America*, 135:2847–2861.